Electronic Supplementary Material (ESI) for ChemComm.

Cu/Cu_2O nanocrystals for electrocatalytic carbon dioxide reduction to multi-carbon products

Yisen Yang,[a,b] Zhonghao Tan,[a,b] Sha Wang,[a,b] Yanyue Wang,[a,b] Jingyang Hu,[a,b] Zhuizhui Su,[a,b] Yingzhe Zhao,[a,b] Jing Tai,[a] and Jianling Zhang*[a,b]

a *Beijing National Laboratory for Molecular Sciences, CAS Key Laboratory of Colloid, Interface and Chemical Thermodynamics, CAS Research/Education Center for Excellence in Molecular Sciences, Institute of Chemistry, Chinese Academy of Sciences, Beijing 100190 (P. R. China)*
E-mail: zhangjl@iccas.ac.cn
b *School of Chemical Sciences, University of Chinese Academy of Sciences, Beijing 100049 (P. R. China)*

Experimental Sections

Materials: Potassium sulfate (K_2SO_4, 99%), potassium phosphate (K_2HPO_4, 98%), potassium bicarbonate ($KHCO_3$, 99.5%), copper chloride dihydrate ($CuCl_2{\cdot}2H_2O$, ≥ 99%), commercial cuprous oxide (Cu_2O), Cu foil, dimethylamine borane (DMAB, 98%), deuterated water (D_2O, 99.9%) and dimethyl sulfoxide (DMSO, 99.0%) were purchased from Beijing InnoChem Science & Technology Co., Ltd. Carbon dioxide (CO_2, 99.999%), Argon (Ar, 99.999%) and deionized (DI) water were supplied by Beijing Analysis Instrument Factory. Methanol (CH_3OH) was provided by Beijing Chemical works. Nafion D-521 dispersion (5% w/w in water and 1-propanol, ≥ 0.92 meq g^{-1} exchange capacity), Nafion N-117 membrane and Toray carbon paper (TGP-H-060) were purchased from Alfa Aesar China Co., Ltd. All reagents were used directly without further treatment.

Synthesis of Cu/Cu_2O nanocrystals: Cu/Cu_2O nanocrystals were synthesized by a wet-chemical method. First, 4 mL of 1 M $CuCl_2{\cdot}2H_2O$ aqueous solution was added to 10 mL of DI water. Then, 4 mL of 1 M DMAB aqueous solution was added dropwise to above solution. After 3 h reaction at 25 °C and air atmosphere, the product was separated by suction filtration, washed several times by copious deionized water and dried in vacuum at 60 °C overnight.

Characterizations: X-ray diffraction (XRD) was determined by a Rigaku D/max-2500 X-ray diffractometer (Rigaku Corporation, Tokyo, Japan) with Cu Kα radiation at 40 kV and 200 mA. The morphologies were characterized by scanning electron microscopy (SEM, Hitachi S-4800) equipped with energy dispersive X-ray elemental (EDX) mapping, transmission electron microscopy (TEM, JEOL-1011) and high-resolution TEM (HRTEM, JEOL-2100F). Fourier transform infrared (FT-IR) spectroscopy was performed by a Bruker Tensor 27 spectrometer. X-ray photoelectron spectroscopy (XPS) was determined by a Thermo Fisher Scientific ESCALAB 250Xi (Thermo Fisher Scientific, Waltham, MA, USA) using 200 W Al Kα radiation. X-ray absorption fine structure (XAFS) data were collected at 1W2B station at Beijing Synchrotron Radiation Facility (BSRF, Beijing, China).

Electrochemical tests: All electrochemical tests were carried out in H-cell by using a CHI660E electrochemical workstation. Before each electrochemical experiment, electrolyte was saturated with CO_2 for at least 40 min. The hydrophobic carbon paper (1 × 0.5 cm^{-2}) coated with catalyst was used as working electrode. Ag/AgCl electrode and Pt net (1 × 1cm^{-2}) were used as reference electrode and counter electrode, respectively. For the preparation of working electrode, 10 mg of catalyst, 40 μL of Nafion D-521 dispersion and 760 μL of CH_3OH were mixed to form the catalyst ink. The ink was then dropcasted onto carbon paper to ensure the loading of 0.75 mg cm^{-2}. The flow rate of CO_2 was adjusted to be 20 mL min^{-1} by gas flow meter.
Because K_2SO_4 aqueous solution does not have buffering capacity, the pH value changes dynamically with time during electrolysis. Therefore, Ag/AgCl scale instead of reversible hydrogen electrode scale was used for all potentials in this article.

Product analysis: For gaseous products, 2 mL of gas extracted from gas bag was injected to gas chromatography (GC, Agilent 8890; Agilent Technologies Inc., CA, USA) with a thermal conductivity detector (TCD) detector using high purity Ar as carrier gas. For liquid products, 200 μL of electrolyte, 200 μL of D_2O and 100 μL of 6 mM DMSO solution were mixed and then detected by ^1H nuclear magnetic resonance (^1H NMR, Bruker AVANCE III 400 HD; Bruker, Germany). The Faradaic efficiency (FE) was calculated by the following formulation:

$$FE = \frac{Moles\ of\ product * n * F}{Q} * 100\%$$

(Q: charge (C); n: the number of electrons required to generate the product; F: Faraday constant (96485 C/mol)).

In situ Raman spectroscopy: In situ Raman spectroscopy was carried out by using a Horiba LabRAM HR Evolution Raman microscope (HORIBA Scientific, Paris, France). The laser wavelength was controlled at 785 nm. 0.10 M K_2SO_4 aqueous solution was used as electrolyte. The gas diffusion layer (YLS-30T) coated with catalyst, Ag/AgCl electrode and carbon rod were used as working electrode, reference electrode and counter electrode, respectively. The in situ Raman electrolytic cell was purchased from Gaoss Union (Tianjin) Photoelectric Technology Company (Tianjin, China).

Results and Discussion

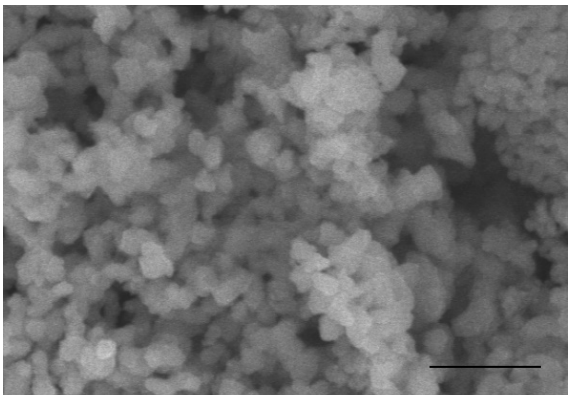

Fig. S1 (a) SEM image of Cu/Cu_2O nanocrystals. (b) Size histogram (>100 particles) of Cu/Cu_2O nanocrystals by analysing SEM image (Fig. 1b) statistically. Scale bar: 500 nm in a.

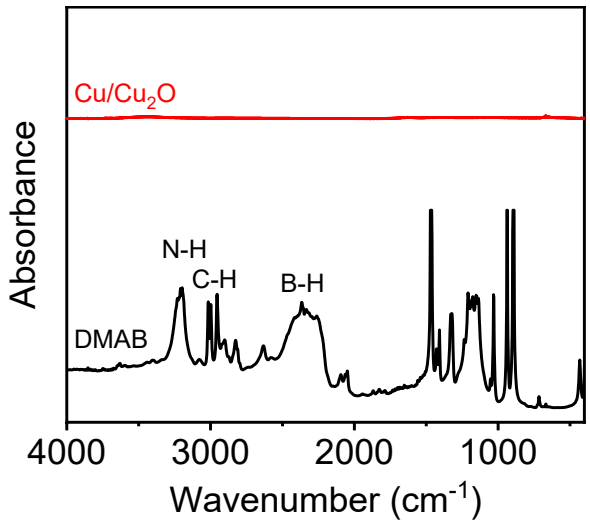

Fig. S2 FT-IR spectra of Cu/Cu_2O nanocrystals and DMAB. The characteristic vibrations of DMAB were not detected in Cu/Cu_2O nanocrystals,[1] indicating its complete removement.

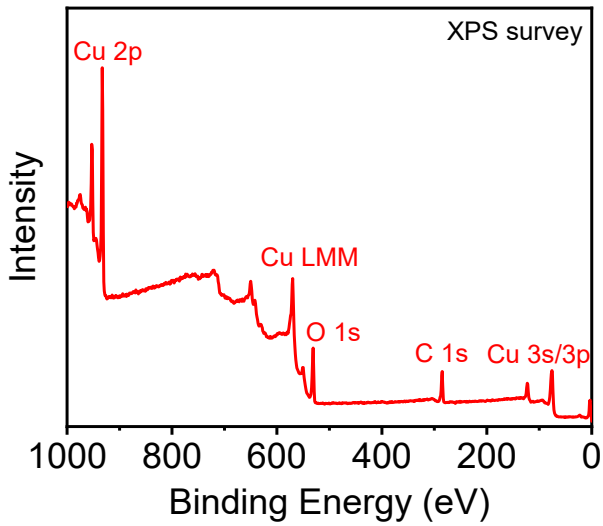

Fig. S3 XPS survey of Cu/Cu_2O nanocrystals.

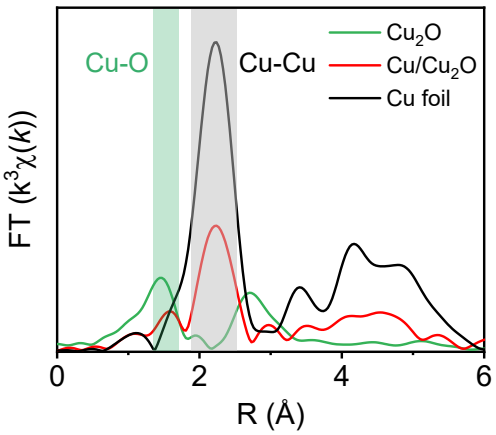

Fig. S4 The k^3-weighted Fourier-transformed extended X-ray absorption fine structure spectra of Cu/Cu_2O nanocrystals, Cu foil and commercial Cu_2O.

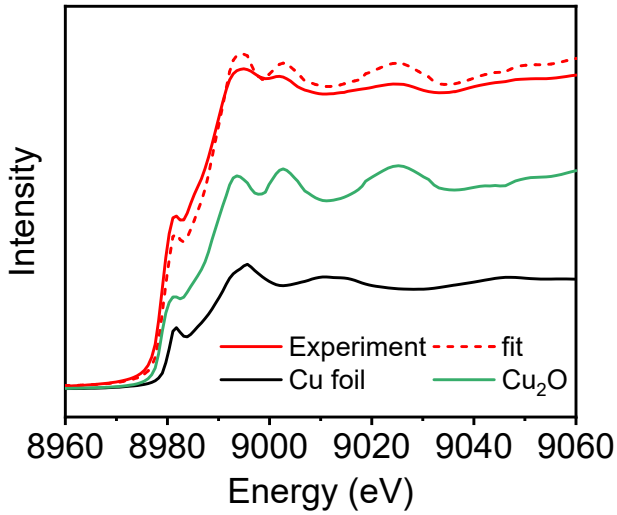

Fig. S5 Cu K-edge X-ray absorption near-edge structure linear combination fitting of Cu/Cu_2O nanocrystals.

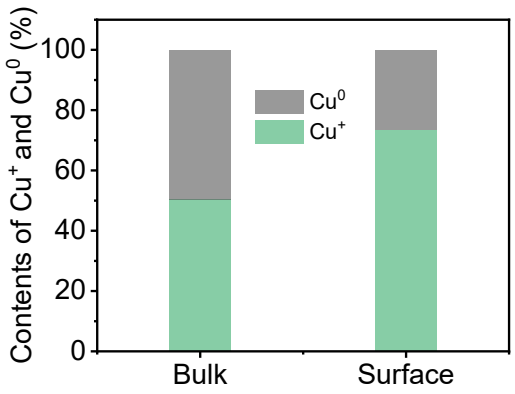

Fig. S6 Contents of Cu^{+} and Cu^{0} in bulk and surface.

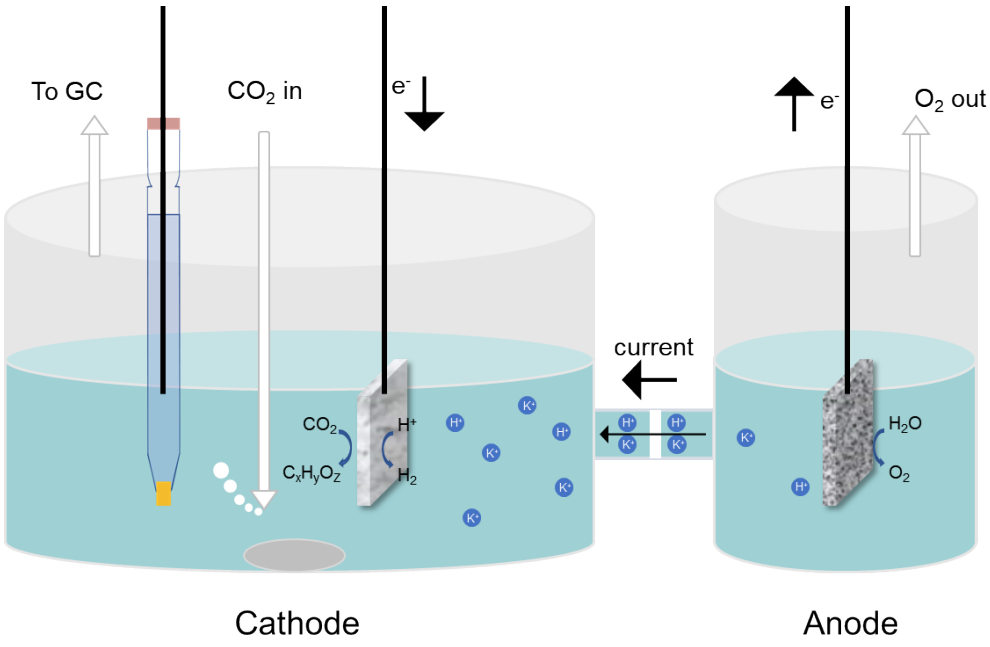

Fig. S7 Illustration of H-cell used in electrocatalytic CO_2 reduction reaction (ECO_2RR).

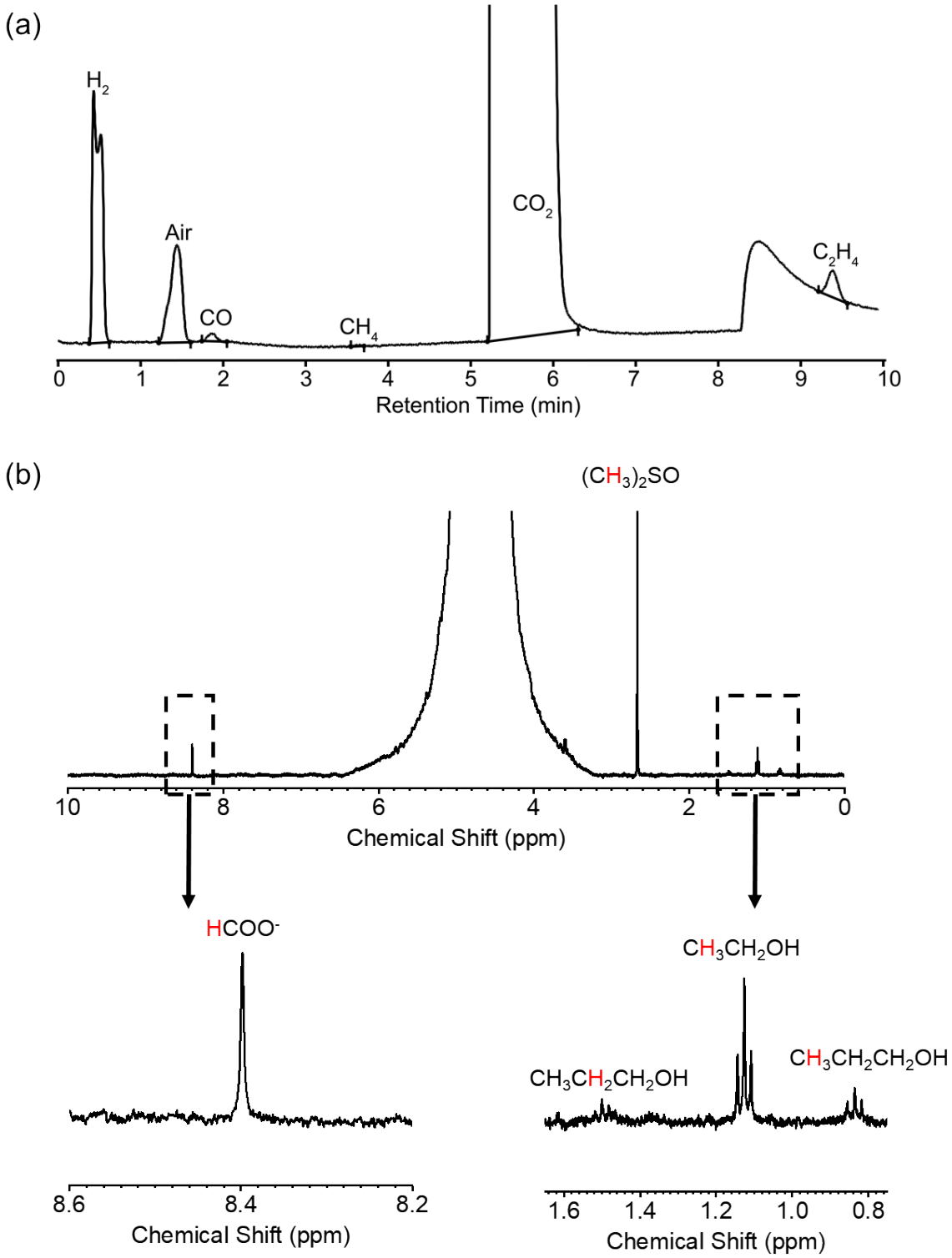

Fig. S8 A typical (a) GC spectrum and (b) ^{1}H NMR spectrum of the products after electrolysis using Cu/Cu_2O nanocrystals.

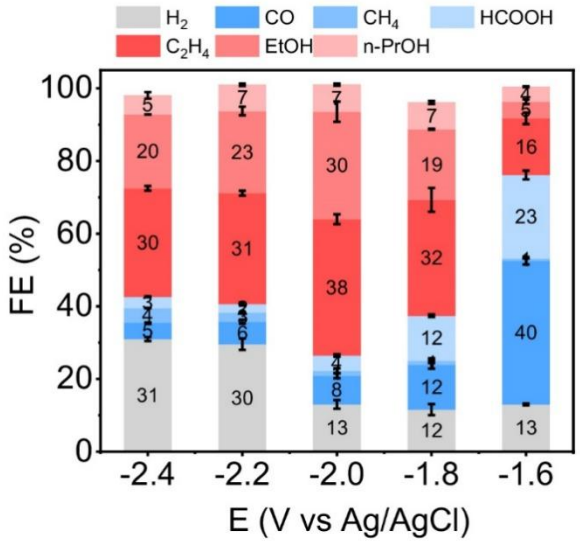

Fig. S9 FE values of all detectable products at potentials ranging from -1.6 to -2.4 V in 0.10 M K_2SO_4.

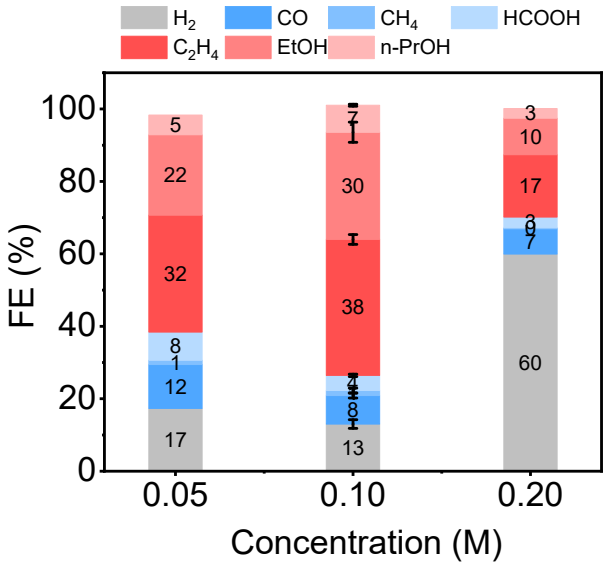

Fig. S10 FE values of all detectable products on Cu/Cu_2O nanocrystals at -2.0 V in 0.05, 0.10 and 0.20 M K_2SO_4.

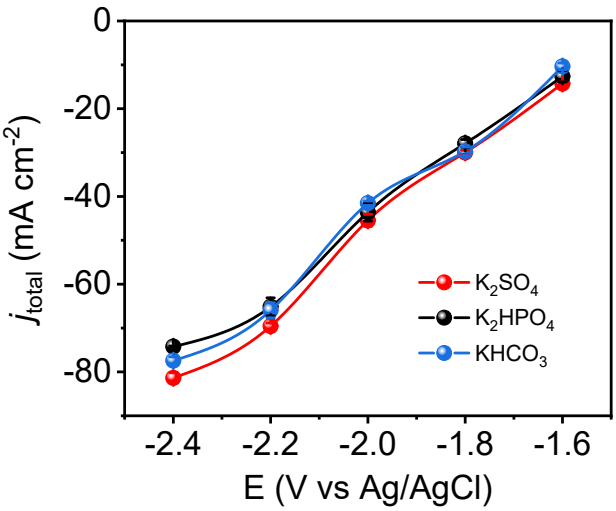

Fig. S11 The total current densities at potentials ranging from -1.6 V to -2.4 V in different electrolytes.

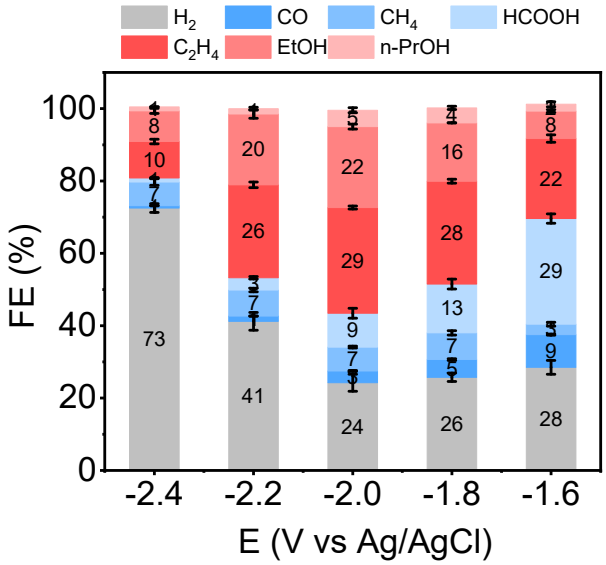

Fig. S12 FE values of all detectable products at potentials ranging from -1.6 to -2.4 V in 0.20 M $KHCO_3$.

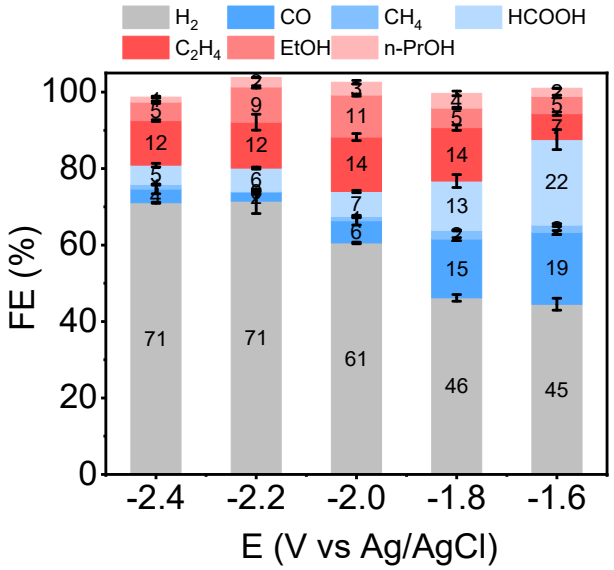

Fig. S13 FE values of all detectable products at potentials ranging from -1.6 to -2.4 V in 0.10 M K_2HPO_4.

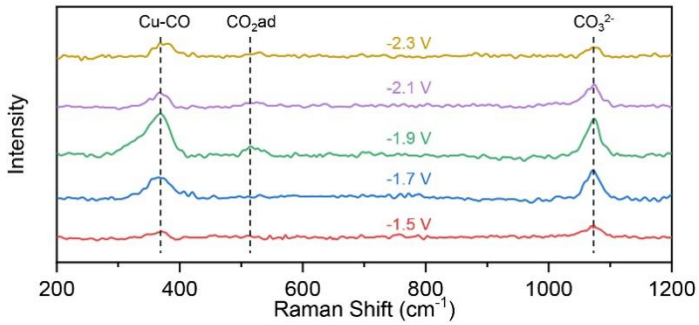

Fig. S14 In situ Raman spectra at various applied potentials.

Table S1. The comparison of multi-carbon products in ECO_2RR on various Cu-based catalysts in H-cell.

Catalysts	FE (%)	Partial current density (mA cm^{-2})	Electrolyte	Reference	Year
Cu/Cu_2O nanocrystals	75.0	34.4	0.1 M K_2SO_4	This work	
Cu/Cu_2O-CV	73.4	~ 4	0.1 M $KHCO_3$	*ACS Catal.*[2]	2022
Cu/Cu_2O aerogel networks	80.8	66.4	0.1 M KCl	*Adv. Funct. Mater.*[3]	2021
Cu/Cu_2O@N-doped graphene	56.0	19.0	0.2 M KI	*J. CO_2 Util.*[4]	2021
Cu@Cu_2O	50	~ 9	0.1 M $KHCO_3$	*J. Colloid Interface Sci.*[5]	2019
IL@Cu	77.2	26.4	0.1 M $KHCO_3$	*Angew. Chem. Int. Ed.*[6]	2022
Dense vertical lamellate Cu	80.5	~ 45	0.5 M KCl	*Nat. Commun.*[7]	2022
Cu-PTFE-nanoneedles	86	53.78	0.1 M $KHCO_3$	*J. Am. Chem. Soc.*[8]	2022
e-CuOHFCl nanosheet	54	~ 10	0.1 M $KHCO_3$	*Angew. Chem. Int. Ed.*[9]	2021
Cu-KI	72.6	29	0.1 M $KHCO_3$	*Nat. Commun.*[10]	2020
Oxygen-bearing Cu micropore nanowires	45	44.7	0.5 M $KHCO_3$	*J. Am. Chem. Soc.*[11]	2020
Nanodefective Cu nanosheet	83.2	48.9	0.1 M K_2SO_4	*J. Am. Chem. Soc.*[12]	2020
Iodine-modified Cu	80	31.2	0.1 M $KHCO_3$	*Angew. Chem. Int. Ed.*[13]	2019
Cu_3N Nanocubes	60	~ 18	0.1 M $KHCO_3$	*Nano Lett.*[14]	2019
Cu-on-Cu_3N	64	25	0.1 M $KHCO_3$	*Nat. Commun.*[15]	2018
100-cycle Cu	60.5	41	0.25 M $KHCO_3$	*Nat. Catal.*[16]	2018

Table S2. The electrical conductivities of 0.10 M K_2SO_4, 0.20 M $KHCO_3$ and 0.10 M K_2HPO_4.

Electrolyte type and concentration	Electrical conductivity (mS cm^{-1})
0.10 M K_2SO_4	18.93
0.20 M $KHCO_3$	17.46
0.10 M K_2HPO_4	16.79

Table S3. Bulk pH values of electrolytes (catholyte): pristine, CO_2-saturated and 100 C-electrolysed at -2.0 V.

Electrolyte type and concentration	Pristine	CO_2-saturated	100 C-electrolysis
0.10 M K_2SO_4	6.0	4.7	6.3
0.20 M $KHCO_3$	8.6	7.1	7.2
0.10 M K_2HPO_4	9.0	6.5	6.7

Supplementary References

1 U. Sanyal and B. R. Jagirdar, *Inorg. Chem.*, 2012, **51**, 13023-13033.
2 Y. Yang, A. He, H. Li, Q. Zou, Z. Liu, C. Tao and J. Du, *ACS Catal.*, 2022, **12**, 12942-12953.
3 C. Kim, K. M. Cho, K. Park, J. Y. Kim, G.-T. Yun, F. M. Toma, I. Gereige and H.-T. Jung, *Adv. Funct. Mater.*, 2021, **31**, 2102142.
4 W. Y. Zhi, Y. T. Liu, S. L. Shan, C. J. Jiang, H. Wang and J. X. Lu, *J. CO_2 Util.*, 2021, **50**, 101594.
5 L. Shang, X. Lv, H. Shen, Z. Shao and G. Zheng, *J. Colloid Interface Sci.*, 2019, **552**, 426-431.
6 Y. Sha, J. Zhang, X. Cheng, M. Xu, Z. Su, Y. Wang, J. Hu, B. Han and L. Zheng, *Angew. Chem. Int. Ed.*, 2022, **61**, e202200039.
7 W. Liu, P. Zhai, A. Li, B. Wei, K. Si, Y. Wei, X. Wang, G. Zhu, Q. Chen, X. Gu, R. Zhang, W. Zhou and Y. Gong, *Nat. Commun.*, 2022, **13**, 1877.
8 B. Yang, K. Liu, H. Li, C. Liu, J. Fu, H. Li, J. E. Huang, P. Ou, T. Alkayyali, C. Cai, Y. Duan, H. Liu, P. An, N. Zhang, W. Li, X. Qiu, C. Jia, J. Hu, L. Chai, Z. Lin, Y. Gao, M. Miyauchi, E. Cortes, S. A. Maier and M. Liu, *J. Am. Chem. Soc.*, 2022, **144**, 3039-3049.
9 M. Li, Y. Ma, J. Chen, R. Lawrence, W. Luo, M. Sacchi, W. Jiang and J. Yang, *Angew. Chem. Int. Ed.*, 2021, **60**, 11487-11493.
10 T. Kim and G. T. R. Palmore, *Nat. Commun.*, 2020, **11**, 3622.
11 W. Zhang, C. Huang, Q. Xiao, L. Yu, L. Shuai, P. An, J. Zhang, M. Qiu, Z. Ren and Y. Yu, *J. Am. Chem. Soc.*, 2020, **142**, 11417-11427.
12 B. Zhang, J. Zhang, M. Hua, Q. Wan, Z. Su, X. Tan, L. Liu, F. Zhang, G. Chen, D. Tan, X. Cheng, B. Han, L. Zheng and G. Mo, *J. Am. Chem. Soc.*, 2020, **142**, 13606-13613.
13 D. Gao, I. Sinev, F. Scholten, R. M. Aran-Ais, N. J. Divins, K. Kvashnina, J. Timoshenko and B. Roldan Cuenya, *Angew. Chem. Int. Ed.*, 2019, **58**, 17047-17053.
14 Z. Yin, C. Yu, Z. Zhao, X. Guo, M. Shen, N. Li, M. Muzzio, J. Li, H. Liu, H. Lin, J. Yin, G. Lu, D. Su and S. Sun, *Nano Lett.*, 2019, **19**, 8658-8663.
15 Z. Q. Liang, T. T. Zhuang, A. Seifitokaldani, J. Li, C. W. Huang, C. S. Tan, Y. Li, P. De Luna, C. T. Dinh, Y. Hu, Q. Xiao, P. L. Hsieh, Y. Wang, F. Li, R. Quintero-Bermudez, Y. Zhou, P. Chen, Y. Pang, S. C. Lo, L. J. Chen, H. Tan, Z. Xu, S. Zhao, D. Sinton and E. H. Sargent, *Nat. Commun.*, 2018, **9**, 3828.
16 K. Jiang, R. B. Sandberg, A. J. Akey, X. Y. Liu, D. C. Bell, J. K. Norskov, K. R. Chan and H. T. Wang, *Nat. Catal.*, 2018, **1**, 111-119.